J. Cent. South Univ. (2020) 27: 381−387
DOI: https://doi.org/10.1007/s11771-020-4303-4

Springer

Microstructure and hot corrosion behavior of Al-Ce-Y coatings on DZ125 nickel-based alloy prepared by pack cementation process

LI Yong-quan(李涌泉), LI Ji-lin(李吉林), QIN Chun(秦春), JIANG Liang(蒋亮), GENG Gui-hong(耿桂宏)

School of Materials Science & Engineering, North Minzu University, Yinchuan 750021, China

Abstract: In order to improve the hot corrosion resistance of DZ125 alloy, Ce-Y modified aluminum coatings were prepared on DZ125 alloy by pack cementation process at 950 °C for 2 h. The microstructure, phase constitution and formation mechanism of the coatings were investigated. The hot corrosion behaviors of DZ125 alloy and the coatings in molten salt environment of 25%K_2SO_4+75%Na_2SO_4 (mass fraction) at 900 °C were studied. Results show that the obtained Al-Ce-Y coatings were mainly composed of Al_3Ni_2, Al_3Ni and Cr_7Ni_3, with a thickness of about 120 μm. After hot corrosion test, DZ125 alloy suffered catastrophic hot corrosion and serious internal oxidation and internal sulfidation arose. Two layers of corrosion products formed on surfaces of DZ125 alloy, including the outer layer consisting of Cr_2O_3 and $NiCr_2O_4$, and the inner layer of Al_2O_3, Ni_3S_2 and Ni-base solid solution. After being coated with Al-Ce-Y coating, the hot corrosion resistance of DZ125 alloy is improved notably, due to the formation of a dense scale mainly consisting of Al-rich Al_2O_3 in the coating layer.

Key words: DZ125 alloy; Ce-Y modified aluminum coating; structure; hot corrosion

Cite this article as: LI Yong-quan, LI Ji-lin, QIN Chun, JIANG Liang, GENG Gui-hong. Microstructure and hot corrosion behavior of Al-Ce-Y coatings on DZ125 nickel-based alloy prepared by pack cementation process [J]. Journal of Central South University, 2020, 27(2): 381−387. DOI: https://doi.org/10.1007/s11771-020-4303-4.

1 Introduction

Nickel-based super alloys are widely used in high temperature applications, such as hot component of gas turbines, aero-engines and boilers for their excellent high-temperature mechanical properties [1]. Furthermore, these components are also subjected to high-temperature oxidation and hot corrosion conditions generated by the combustion environment and fuel consumption [2, 3]. Unfortunately, the requirements regarding high-temperature strength usually conflict with the requirement of hot corrosion resistance of these alloys. A practical solution to this conflict is to develop a protective coating to protect nickel- based super alloys against high-temperature oxidation and hot corrosion [4].

Based on recent researches on oxidation and hot corrosion behavior of nickel-based super alloys, a number of corrosion protective techniques, such as vacuum fusing [5], sputtering deposition [6], pack cementation [7], plasma spray [8] and ion implantation [9], have been proposed. Among these techniques, the pack cementation process is a convenient and effective method to obtain high-performance surface coatings with excellent corrosion and oxidation resistant performance. Aluminizing, chromizing, carburizing and boriding have been successfully carried out by pack cementation process, which is basically an in-situ, self generated chemical vapor deposition (CVD)

Foundation item: Project(51961003) supported by the National Natural Science Foundation of China; Project(NGY2018-148) supported by the Science and Technology Research of Ningxia Colleges, China; Project(NZ16083) supported by Key Program of Natural Science Foundation of Ningxia, China
Received date: 2019-02-26; **Accepted date:** 2019-06-21
Corresponding author: LI Yong-quan, PhD; Tel/Fax: +86-951-2067378; E-mail: 8386595@163.com; ORCID: 0000-0001-6095-8761

process [10].

Due to the formation of a protective Al_2O_3 scale with perfect oxidation resistance at high temperature, aluminum coatings were extensively employed to improve the surface properties of Ti and nickel alloys [11]. In recent years, the oxidation behavior of aluminum coatings has been investigated extensively, while its corrosion resistance performance was rarely reported. Moreover, many researchers have reported that the rare earth elements (Re) have positive influences on reducing the grain size, improving the toughness and enlarging the thickness of the surface coatings. Hot corrosion resistance of surface coatings was improved remarkably by the addition of small amounts of Re [12].

In this work, Ce-Y mollified aluminum coatings were prepared on DZ125 alloy by pack cementation process. The cross-sectional microstructure, elemental distribution and phase constitution of the Al-Ce-Y coating were systematically analyzed. Meanwhile, the hot corrosion behaviors of DZ125 substrate and the Al-Ce-Y coating were investigated. The corrosion mechanisms of DZ125 alloy and the Al-Ce-Y coating were discussed as well.

2 Experimental procedures

The chemical composition of DZ125 alloy used for the experiments was Ni-0.09C-8.9Cr-10.0Co-7.5W-1.6Mo-5.3Al-0.8Ti-3.8Ta-1.5Hf-0.015B (wt.%). The substrate samples were cut into blocks with dimensions of 20 mm×20 mm×3 mm by electro-discharge machining. All the specimens were burnished using SiC-grit papers up to No.1500. The burnished samples were ultrasonically cleaned in alcohol bath and dried before coating.

According to previous research results of our group [13−15], the pack mixture used for the pack process was composed of 15Al-1Y_2O_3-1Ce_2O_3-7NH_4Cl-76Al_2O_3 (wt%; pure Al, Y_2O_3, Ce_2O_3, powders as donor sources, NH_4Cl powder as activator and Al_2O_3 as filler). The powders were weighed and then mixed by tumbling in a ball mill for 4 h. The Al-Ce-Y co-deposition coatings were prepared by burying the DZ125 substrates with the pack mixture in an alumina crucible, which was then sealed with an Al_2O_3-based silica sol binder. Pack cementations were conducted in an electric tube furnace, which was heated to 950 °C at a rate of 15 °C/min. After being held at 950 °C for 2 h, the specimens were furnace cooled to room temperature.

The hot corrosion test of the DZ125 substrates and the Al-Ce-Y coatings were conducted in molten $(Na, K)_2SO_4$ (25% K_2SO_4+75%Na_2SO_4, mass fraction) salt at 900 °C for different time before cooling down in air to room temperature. The salt adhered to surfaces of the samples was dissolved by putting the samples into distilled water. After being dried, the mass changes of the samples after hot corrosion were measured using an electronic balance (accuracy 0.1 mg).

X-ray diffraction analysis (XRD, Panalytical X'Pert PRO) was employed to identify the phases of both coating and hot corrosion specimens. Their cross-sectional microstructure and chemical composition of the constituent phases were analyzed by a scanning electron microscope (SEM, JSM-6360LV) equipped with an energy dispersive spectroscope (EDS).

3 Results and discussion

3.1 Coating structure

Figure 1 shows the cross-sectional BSE image and XRD pattern of Al-Ce-Y coating prepared at 950 °C for 2 h. As can be seen in Figure 1(a), the coating had a uniform and compact microstructure with a total thickness of about 120 μm. The higher magnification morphology inserted in Figure 1(a) showed that an large number of white particles (point 1) uniformly distributed in black (point 2) and grey black matrix (point 3). EDS analysis proved that the white particles had a higher concentration of Cr, W and Ta than the black and grey black matrix, which realizes dispersion strengthening in the coating. Moreover, the contents of Al and Ni in the black and grey black matrix were 64.61 at%, 23.64 at% and 52.78 at%, 40.51 at%. Based on Ni-Al binary phase diagram [16] and XRD pattern (Figure 1(b)), they were Al_3Ni and Al_3Ni_2 respectively. In addition, it was obvious that the contents of Ce and Y in the outer layer of the coating were respectively in the range of 0.67 at%−0.78 at% and 0.71 at%−0.94 at%, and Cr_7Ni_3 phase was also detected in the XRD pattern (Figure 1(b)).

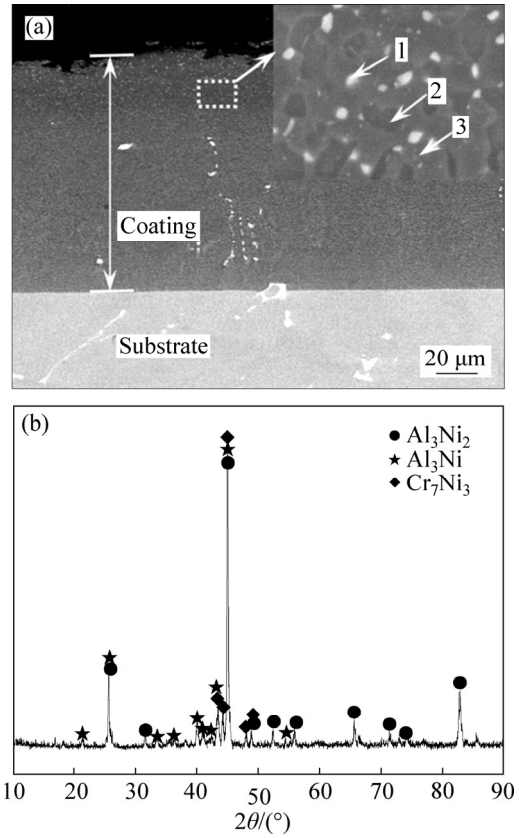

Figure 1 Cross-sectional BSE image (a) and XRD pattern (b) of Al-Ce-Y coating

3.2 Formation mechanism of coating

Pack cementation process is an in situ chemical vapor deposition (CVD) process, and metal-halide vapors of the elements to be deposited are generated via a series of chemical reactions during the pack cementation process, including:

$$NH_4Cl \rightarrow NH_3(g)+HCl(g) \quad (1)$$

$$2NH_3(g) \rightarrow N_2(g)+3H_2(g) \quad (2)$$

$$2M(s)+2xHCl(g)=2MCl_x(g)+xH_2(g) \ (x=1, 2, 3) \quad (3)$$

where M represents Al, Ce or Y element. The chemical potential gradient between the pack mixture and the substrate drove the gas phase diffusion of MCl vapors to the surface of the substrate, and the following reactions might happen:

$$MCl_x(g)+xNi(s)=xNiCl(s)+[M](g) \quad (4)$$

or

$$(x+1)MCl_x(g)=xNiCl_{(x+1)}(g)+[M](s) \quad (5)$$

Therefore, the active [M] atoms were adsorbed on the surface of the alloy and diffused into the DZ125 substrate at high temperature to form the coating. Previous research elucidated that the growth rate of the aluminum coating on nickel base alloy was controlled by the inward diffusion of Al element [17]. The appearance of white particles (point 1) in the coating was caused by the segregation of Cr and W atoms, which has a low solid solubility in NiAl phase. Moreover, active Ce and Y atoms would be adsorbed on the surface and polarize for micro and macro-inhomogeneity of the coating's surface ($(k+n+1)RE \leftrightarrow RE^{3+}+kRE^{2+}+nRE^{+}+(2k+n+3)e$)) [18]. This produced active center and increased the adsorption of active Al atoms, which resulted in higher chemical potential and diffusion rate of Al. Meanwhile, rare earth Ce and Y elements with large radius will preferentially occupy the grain boundary position and lattice defects during the process of the coating formation, and cause lattice distortion around them, which also increased the adsorption of active Al atoms. Therefore, thicker coatings were obtained. In addition, Ce and Y elements mainly existed in the outer layer of the Al-Ce-Y coatings with relatively lower content. This is due to the high activation energy required for Y element diffusion, which was related to its high melting point (T_m) of 1799 K according to the empirical equation $Q=32T_m$ [19]. For Ce element, its melting point is low (1071 K) and its atomic radius is larger (2.7 nm) than that of Y (2.27 nm) and Al (1.82 nm), which hinders its diffusion towards the coating. Therefore, the contents of Ce and Y elements in the coating were lower.

3.3 Hot corrosion behavior of Al-Ce-Y coating

3.3.1 Corrosion kinetics

Figure 2 shows the corrosion kinetics of DZ125 alloy and Al-Ce-Y coating in $(Na, K)_2SO_4$ melt. As shown in Figure 2, the mass gains of the DZ125 alloy and Al-Ce-Y coating were about 1.03, 0.42 mg/cm^2 after 20 min hot corrosion, respectively. With increasing corrosion time, the mass gain of DZ125 alloy increased to 23.45 mg/cm^2 after being hot corroded for 120 min and then decreased remarkably. However, the mass gain of Al-Ce-Y coating increased slightly during the experiment. From the above results, it can be deduced that the corrosion products on surfaces of DZ125 alloy do not provide complete protection for the DZ125 substrate, and the hot corrosion resistance of the coating is better than that of

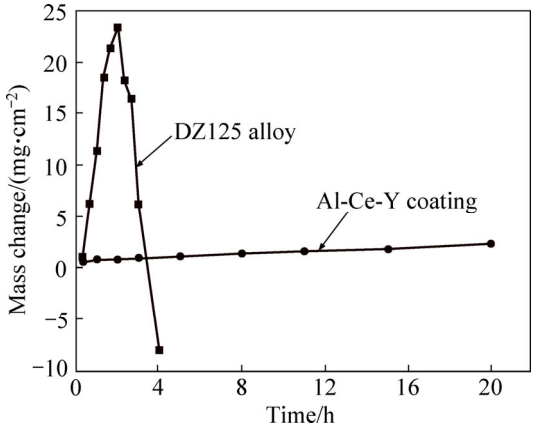

Figure 2 Corrosion kinetics of DZ125 alloy and Al-Ce-Y coating in (Na, K)$_2$SO$_4$ melt

substrate. It should be emphasized that some corrosion products will inevitably flake off during the process of cleaning the residual salt on the alloy surface after thermal corrosion in the test. Therefore, there is a large error in evaluating the thermal corrosion resistance of the alloy through the weight loss and weight gain curves obtained by this method.

3.3.2 Hot corrosion scale morphologies

Figure 3 shows the surface morphology and XRD pattern of the DZ125 alloy after hot corrosion in (Na, K)$_2$SO$_4$ melt at 900 °C for 2 h. As shown in Figure 3(a), it can be seen that the hot corrosion scale formed on the surface is loose with cracks. EDS analyses revealed that the contents of Cr and S in the surface of the scale were about 18.65 at.% and 4.66 at.% respectively. According to the XRD patterns (Figure 3(b)), the hot corrosion scale was determined to be mainly composed of NiSS (Ni-based solid solution), $NiCr_2O_4$ and Cr_2O_3 phases. It should be noted that the diffraction peaks representing Ni_3S_2 and Al_2O_3 phases were also observed in Figure 3(b), which is due to exposure of the inner layer of the corrosion product caused by the partial shedding of the corrosion product.

Figure 4 shows the cross-sectional BSE image of the DZ125 alloy after hot corrosion in (Na, K)$_2$SO$_4$ melt at 900 °C for 2 h (when the hot corrosion time was longer than 2 h, the hot corrosion scale formed on the DZ125 alloy flaked off during the salt cleaning process). It can be seen that the hot corrosion film had a porous structure with a total thickness of about 190 μm, and there is a discontinuous fracture zone in the middle of the corrosion film. EDS analysis results revealed that

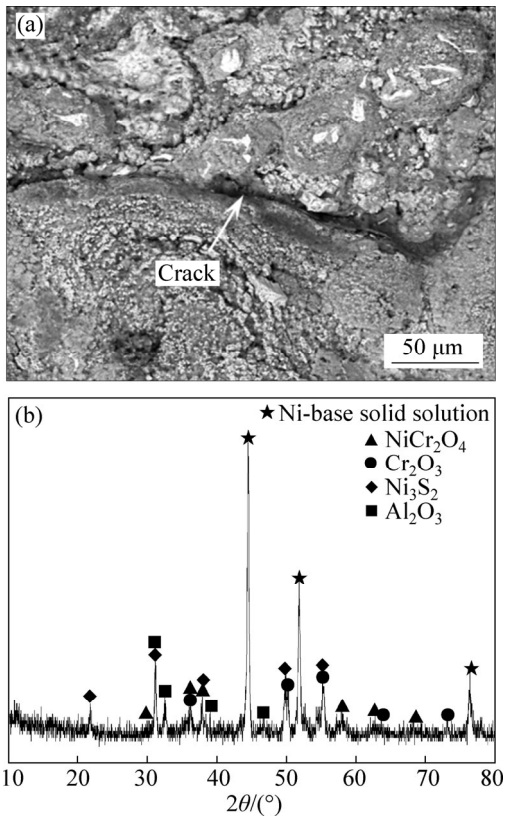

Figure 3 Surface morphology of DZ125 alloy after hot corrosion in (Na, K)$_2$SO$_4$ melt at 900 °C for 2 h (a) and XRD pattern of scale (b)

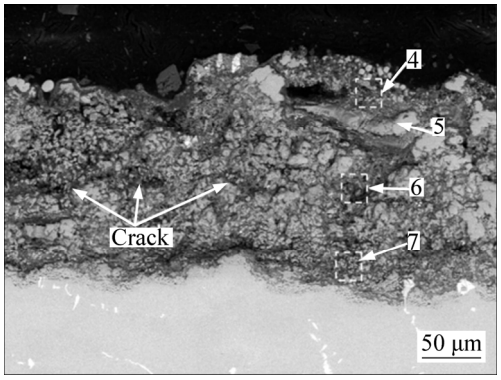

Figure 4 Cross-sectional morphology of DZ125 alloy after hot corrosion in (Na, K)$_2$SO$_4$ melt at 900 °C for 2 h

the black tissue in the outer layer of corrosion film (Figure 4, point 4) had a composition of 12.68O-7.66S-48.3Cr-4.88Co-16.23Ni-3.99Al-4.11Ti-2.15Ta (at.%). According to the XRD pattern (Figure 3(b)), the black tissue was determined to be $NiCr_2O_4$ and Cr_2O_3. Beneath the black tissue, numerous blocky and gray tissues (point 5) were detected. EDS analyses revealed that the contents of Ni and Co in the gray tissue were about 18.65 at% and 4.66 at% respectively, and the gray tissue was determined to be Co-rich NiSS. In addition, the

contents of Al and S in the fracture zone (Figure 4, point 6) were 35.07 at% and 12.18 at.%, and it was confirmed to consist of Al_2O_3 and Ni_3S_2 phases according to the XRD patterns (Figure 3(b)). The inner layer (Figure 4, point 7) of the corrosion film had a composition of 10.28O-2.6S-55.95Cr-5.31Co-14.68Ni-4.49Al-3.25Ti-3.44Ta (at.%), which was similar with that of the outer layer of the corrosion film, predicating the beginning of a new corrosion process.

Figure 5 shows the surface morphologies and XRD patterns of the Al-Ce-Y coating after hot corrosion in $(Na,K)_2SO_4$ melt at 900 °C for 20 h. It was found that the coating had a compact and dense film after 20 h hot corrosion, as shown in Figure 5(a). Figure 5(b) indicates that the corrosion film was composed of Al_2O_3, Al_3Ni_2 and NiAl phases.

Figure 6 shows the cross-sectional BSE image of the Al-Ce-Y coating after hot corrosion in $(Na,K)_2SO_4$ melt at 900 °C for 20 h. A hot corrosion film with a thickness of 10−15 μm formed on the surface of the coating. EDS analysis revealed that the black tissues (Figure 6, point 8) of the corrosion film had a composition of 22.62O-2.36S-5.23Ni-69.79Al (at.%), which was confirmed to consist of Al-rich Al_2O_3 phase. As the Al-rich Al_2O_3 film is compact and well combined with the remained coating, the hot corrosion resistance of the coating was significantly improved due to inhibition of the diffusion of O and S elements.

3.3.3 Hot corrosion mechanism

Both sulfides and oxides were detected in the corrosion products of DZ125 alloy in $(Na, K)_2SO_4$ molten salt contained. Since it was difficult for external O and S elements to enter the corrosion system, the O and S elements mainly resulted from the high-temperature decomposition of Na_2SO_4 through the following thermodynamic equilibrium existing in the corrosion system [20]:

$$Na_2SO_4 \rightarrow Na_2O+SO_2+1/2O_2 \quad (6)$$

$$K_2SO_4 \rightarrow K_2O+SO_2+1/2O_2 \quad (7)$$

Actually, the molten salt is a high-sulfur, low-oxygen potential system.

The content of Cr in DZ125 alloy is higher than that of Al, and the Cr element has the better short-circuit diffusion ability along the grain

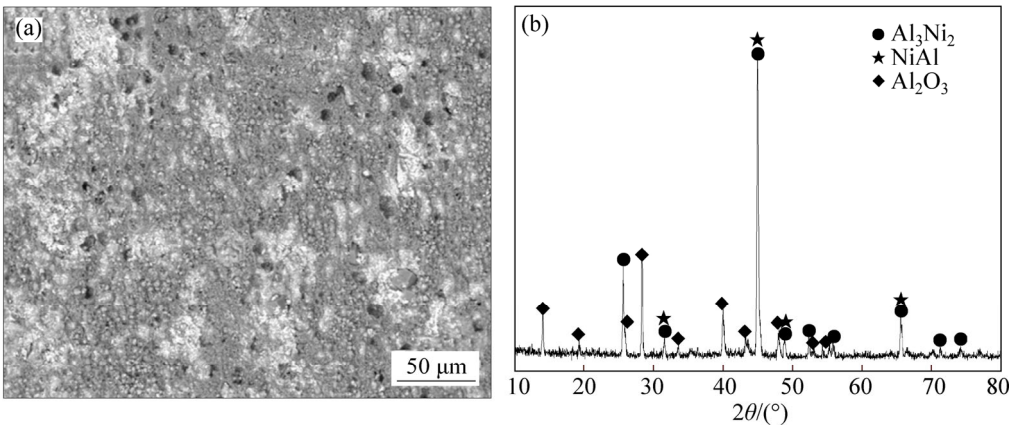

Figure 5 Surfaces morphologies of Al-Ce-Y coating after hot corrosion in $(Na,K)_2SO_4$ melt at 900 °C for 20 h (a) and XRD pattern of scale (b)

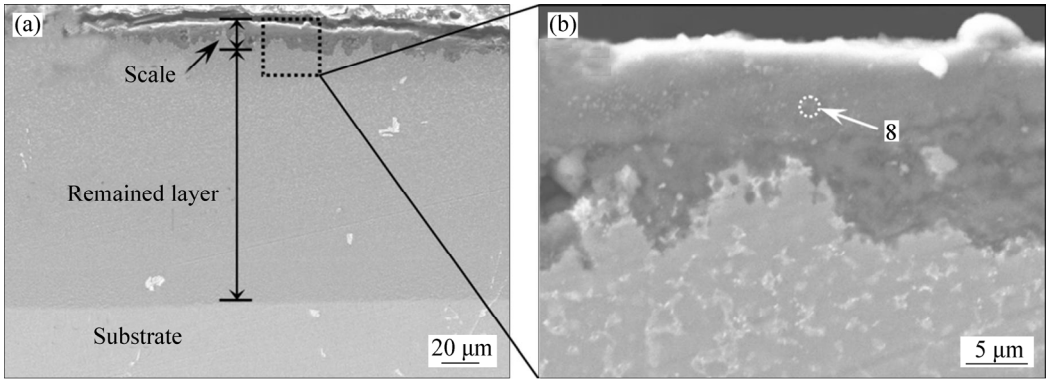

Figure 6 Cross-sectional morphologies of Al-Ce-Y coating after hot corrosion in $(Na, K)_2SO_4$ melt at 900 °C for 20 h

boundaries compared with other elements. Moreover, refractory elements such as W, Mo reduced the migration rate of Al element. Hence, a mixed oxide film mainly is composed of Cr_2O_3 formed on the surface of DZ125 alloy firstly during the hot corrosion process. However, the content of Cr in DZ125 alloy is insufficient to form a compact and dense Cr_2O_3 oxidation film, which leads to the inner diffusion along grain boundaries of O and S elements. With an outward growth of Cr_2O_3, an Al rich layer was developed in the corrosion film beneath the Cr_2O_3 scale, and thus an Al_2O_3 dominated layer formed. With the formation of Al_2O_3 and Cr_2O_3, O element was consumed and the S content in the system was relatively increased, which resulted in the reaction of S and Ni and formation of Ni_3S_2:

$$3Ni+2S\rightarrow Ni_3S_2 \quad (8)$$

During the chemical reactions, an low-melting-point eutectic of Ni-Ni_3S_2 formed (melting point: 625−695 °C), which could lead to the cracking of corrosion film under stresses (Figure 4). The cracked corrosion film partially flaked off, leaving the remaining loose corrosion film as rapid diffusion channels of O and S elements. Therefore, as the corrosion continues, a new cycle of thermal corrosion begins.

The aluminum content in the Al-Ce-Y coating is higher, and the formation enthalpy of Al_2O_3 is lower than that of NiO (−869.04 and −267 kJ/mol respectively). So, the oxidation of Al element occurred prior to the oxidation of Ni during the hot corrosion, resulting in the formation of a compact and dense Al_2O_3 film which prevented the inward diffusion of O and S. Moreover, the Ce and Y elements have been reported to be beneficial in improving the adhesion of the corrosion film [21]. Therefore, the Al-Ce-Y coating provided good protection for DZ125 alloy during hot corrosion in $(Na, K)_2SO_4$ melt at 900 °C.

4 Conclusions

1) A uniform and compact Al-Ce-Y coating with a total thickness of about 120 μm was prepared at 950 °C for 2 h, consisting of Al_3Ni_2, Al_3Ni and Cr_7Ni_3 phases.

2) The hot corrosion film of DZ125 alloy in the salt of $(Na, K)_2SO_4$ was mainly composed of Cr_2O_3, $NiCr_2O_4$ in the outer layer, and Al_2O_3 and Ni_3S_2 in the inner layer. Internal oxidation and sulfidation were main reasons that caused the failure of DZ125 alloy.

3) The Al-Ce-Y coatings possess excellent hot corrosion resistance in the mixture salt of $(Na, K)_2SO_4$ due to inhibition of inward diffusion of O and S by Al_2O_3 scale.

References

[1] YANG F B, JING Y H, LI D. Microstructure and mechanical property of MIM 418 superalloy [J]. Rare Metals, 2018, 37(1): 35−40. DOI: 10.1007/s12598-014-0419-8.

[2] CHANG J X, WANG D, LIU X G, LOU L H, ZHANG J. Effect of rhenium addition on hot corrosion resistance of Ni-based single crystal superalloys [J]. Metallurgical and Materials Transactions, 2018, 49: 4343−4352. DOI: 10.1007/s11661-018-4711-3.

[3] ZHOU Hong-ming, HU Xue-yi, LI Jian. Corrosion behaviors and mechanism of electroless Ni-Cu-P/n-TiN composite coating [J]. Journal of Central South University, 2018, 25(6): 1350−1357. DOI: https://doi.org/10.1007/s11771-018-3831-7.

[4] LIU Zong-jie, ZHOU Chun-gen. Hot corrosion behavior of Si-Y-Co-modified aluminide coating exposed to NaCl+Na_2SO_4 salt at 1173 K [J]. Oxidation of Metals, 2016, 85: 205−217. DOI: 10.1007/s11085-015-9599-3.

[5] ZHOU W, ZHAO Y G, QIN Q D. A new way to produce Al-Cr coating on Ti alloy by vacuum fusing method and its oxidation resistance [J]. Materials Science and Engineering A, 2006, 430: 254−259. DOI: 10.1016/j.msea.2006.05.101.

[6] KIM N H, SEONGHA O, LEE W S. Non-selenization method using sputtering deposition with a $CuSe_2$ target for CIGS thin film [J]. Journal of the Korean Physical Society, 2012, 61(8):1177−1180. DOI: 10.3938/jkps.61.1177.

[7] LIN Nai-ming, ZHAO Lu-lu, LIU Qiang, ZOU Jiao-juan, XIE Rui-zhen, YUAN Shuo, LI Da-li, ZHANG Lu-xia, WANG Zhi-hua, LIU Xiao-ping, TANG Bin. Preparation of titanizing coating on AISI 316 stainless steel by pack cementation to mitigate surface damage: Estimations of corrosion resistance and tribological behavior[J]. Journal of Physics and Chemistry of Solids, 2019, 129: 387−400. DOI: 10.1016/j.jpcs.2019.01.029.

[8] BISHOY A, PATRICK G, CHRISTIAN M. Erratum to: Temperature measurement challenges and limitations for in-flight particles in suspension plasma spraying [J]. Journal of Thermal Spray Technology, 2017, 26(4): 798−804. DOI: 10.1007/s11666-017-0543-8.

[9] LIN Nai-ming, HUANG Xiao-bo, ZHANG Xiang-yu, FAN Ai-lin, QIN Lin, TANG Bin. In vitro assessments on bacterial adhesion and corrosion performance of TiN coating on Ti6Al4V titanium alloy synthesized by multi-arc ion plating [J]. Applied Surface Science, 2012, 258: 7047−7051. DOI: 10.1016/j.apsusc.2012.03.163.

[10] STATHOKOSTOP D, CHALIAMPALISA D, TARANI E. Formation of the thermoelectric candidate chromium

silicide by use of a pack-cementation process [J]. Journal of Electronic Materials, 2014, 43(10): 3733−3739. DOI: 10.1007/s11664-014-3100-y.

[11] ZHANG Ping, GUO Xi-ping. A comparative study of two kinds of Y and Al modified silicide coatings on an Nb-Ti-Si based alloy prepared by pack cementation technique [J]. Corrosion Science, 2011, 53(12): 4291−4299. DOI: 10.1016/j. corsci.2011.08.040.

[12] LIN N M, XIE F Q, ZHOU J. Microstructures and wear resistance of chromium coatings on P110 steel fabricated by pack cementation [J]. Journal of Central South University of Technology, 2010, 17: 1144−1162. DOI: 10.1007/s11771-010-0612-3.

[13] LI Yong-quan, XIE Fa-qin, WU Xiang-qing, LI Xuan. Effects of Y_2O_3 on the microstructures and wear resistance of Si-Al-Y co-deposition coatings prepared on TiAl alloy by pack cementation technique [J]. Applied Surface Science, 2013, 278: 30−36. DOI: 10.1016/j.apsusc.2013.09.050.

[14] LI Yong-quan, XIE Fa-qin, WU Xiang-qing. Microstructure and high temperature oxidation resistance of Si-Y co-deposition coatings prepared on a TiAl alloy by pack cementation process [J].Transactions of Nonferrous Metals Society of China, 2015, 25: 803−807. DOI: 10.1016/S1003-6326(15)63666-4.

[15] LI Yong-quan, XIE Fa-qin, WU xiang-qing. Si-Al-Y Co-deposition coatings prepared on Ti-Al alloy for enhanced high temperature oxidation resistance [J]. Journal of Wuhan University of Technology-Mater, 2018, 33(4): 959−966. DOI: 10.1007/s11595-018-1919-4.

[16] HUNZIKER O, KU W. Drectional solidification and phase equilibria in the Ni-Al system [J]. Metallurgical and Materials Transactions A, 1999, 30: 3167−3172. DOI: 10.1007/s11661-999-0227-1.

[17] XIANG Z D, DATTA P K. Aluminide coating formation on nickel-base superalloys by pack cementation process [J]. Journal of Materials science, 2001, 36: 5673−5682. DOI: 10.1023/a:1012534220165.

[18] ZHANG J Z, YANG Z L, WEI K Y. Study of the catalysis and diffusion mechanism by rare earth (RE) elements during the thermo-chemical treatment [J]. Materials Review, 2006, 20: 223−225. DOI: 10.3321/j.issn:1005-023X.2006.z1. 072

[19] LI Xuan, GUO Xi-ping, QIAO Yan-qiang. Friction and wear behaviors of Nb-Ti-Si-Cr based ultrahigh temperature alloy and its Zr-Y jointly modified silicide coatings [J]. Transactions of Nonferrous Metals Society of China, 2016, 26: 1892−1901. DOI: 10.1016/S1003-6326(16)64267-X.

[20] WU Duo-li, JIANG Su-meng, QI Xiang, GONG Fan-jun, SUN Chao. Hot corrosion behavior of a Cr-modified aluminide coating on a Ni-based superalloy [J]. Acta Metallurgica Sinica, 2014, 27(4), 627−634. DOI: 10.1007/s40195-014-0108-5.

[21] ZHANG Ping, GUO Xi-pin. Y and Al modified silicide coatings on an Nb-Ti-Si based ultrahigh temperature alloy prepared by pack cementation process [J]. Surface and Coatings Technology, 2011, 206(2): 446−454. DOI: 10.1016/j.surfcoat.2011.07.056.

(Edited by YANG Hua)

中文导读

DZ125 镍基合金表面 Al-Ce-Y 渗层的组织及抗热腐蚀性能

摘要：采用扩散渗方法在 DZ125 合金表面制备了 Al-Ce-Y 渗层。分析了渗层的组织结构和形成机制，对比研究了 DZ125 合金基体及渗层在 900 °C 的 25%K_2SO_4+75%Na_2SO_4 熔盐（质量分数 wt. %）中的热腐蚀行为，探讨了其腐蚀速率和腐蚀机理。结果表明：经 950 °C 保温 2 h 所制备的 Al-Ce-Y 渗层厚约 120 μm，主要由 Al_3Ni_2、Al_3Ni 和少量 Cr_7Ni_3 相组成。在 K_2SO_4+Na_2SO_4 熔盐中，DZ125 合金腐蚀产物膜分为两层，外层主要为 Cr_2O_3 和 $NiCr_2O_4$，内层主要为 Al_2O_3、Ni_3S_2 和镍基固溶体，内氧化和内硫化是其失效的主要原因；Al-Ce-Y 渗层在热腐蚀的过程中，渗层表面形成了致密的富 Al 的 Al_2O_3 膜层，显著提高了 DZ125 合金的抗热腐蚀性能。

关键词：DZ125 合金；Ce-Y 改性渗铝涂层；组织；热腐蚀